J Physiol 595.22 (2017) pp 6993–7008

The Journal of Physiology

Leukoencephalopathy-causing *CLCN2* mutations are associated with impaired Cl^- channel function and trafficking

Héctor Gaitán-Peñas[1,2], Pirjo M Apaja[3,4,5], Tanit Arnedo[1,2], Aida Castellanos[6], Xabier Elorza-Vidal[1,2], David Soto[6], Xavier Gasull[6], Gergely L Lukacs[3,4] and Raúl Estévez[1,2]

[1]*Unitat de Fisiología, Departament de Ciències Fisiològiques, IDIBELL-Institute of Neurosciences, Universitat de Barcelona, L'Hospitalet de Llobregat, Spain*
[2]*Centro de Investigación en Red de Enfermedades Raras (CIBERER), ISCIII, Spain*
[3]*Department of Physiology, McGill University, Montréal, Quebec, H3E 1Y6, Canada*
[4]*Research Group Focused on Protein Structure, McGill University, Montréal, Quebec, H3E 1Y6, Canada*
[5]*South Australian Health and Medical Research Institute, Nutrition and Metabolism Theme and EMBL Australia, 5000, Adelaide, Australia*
[6]*Neurophysiology Laboratory, Physiology Unit, Department of Biomedicine, Medical School, Institute of Neurosciences, IDIBAPS, University of Barcelona, Barcelona, Spain*

Key points

- Characterisation of most mutations found in *CLCN2* in patients with CC2L leukodystrophy show that they cause a reduction in function of the chloride channel ClC-2.
- GlialCAM, a regulatory subunit of ClC-2 in glial cells and involved in the leukodystrophy megalencephalic leukoencephalopathy with subcortical cysts (MLC), increases the activity of a ClC-2 mutant by affecting ClC-2 gating and by stabilising the mutant at the plasma membrane.
- The stabilisation of ClC-2 at the plasma membrane by GlialCAM depends on its localisation at cell–cell junctions.
- The membrane protein MLC1, which is defective in MLC, also contributes to the stabilisation of ClC-2 at the plasma membrane, providing further support for the view that GlialCAM, MLC1 and ClC-2 form a protein complex in glial cells.

Abstract Mutations in *CLCN2* have been recently identified in patients suffering from a type of leukoencephalopathy involving intramyelinic oedema. Here, we characterised most of these mutations that reduce the function of the chloride channel ClC-2 and impair its plasma membrane (PM) expression. Detailed biochemical and electrophysiological analyses of the Ala500Val mutation revealed that defective gating and increased cellular and PM turnover contributed to defective A500V-ClC-2 functional expression. Co-expression of the adhesion molecule GlialCAM, which forms a tertiary complex with ClC-2 and megalencephalic leukoencephalopathy with subcortical cysts 1 (MLC1), rescued the functional expression of the mutant by modifying its gating properties. GlialCAM also restored the PM levels of the channel by impeding its turnover at the PM. This rescue required ClC-2 localisation to cell–cell junctions, since a GlialCAM mutant with compromised junctional localisation failed to rescue the impaired stability of mutant ClC-2 at the PM. Wild-type, but not mutant, ClC-2 was also stabilised by MLC1 overexpression. We suggest that leukodystrophy-causing *CLCN2* mutations reduce the functional expression of ClC-2, which is partly counteracted by GlialCAM/MLC1-mediated increase in the gating and stability of the channel.

H. Gaitán-Peñas and P. M. Apaja contributed equally to this study.

DOI: 10.1113/JP275087

(Resubmitted 8 August 2017; accepted after revision 11 September 2017; first published online 14 September 2017)
Corresponding author R. Estévez: Facultat de Medicina, Departament de Ciències Fisiològiques, IDIBELL-Universitat de Barcelona, C/Feixa Llarga s/n 08907, L'Hospitalet de Llobregat, Barcelona, Spain. Email: restevez@ub.edu

Abbreviations CC2L, *CLCN2*-related leukoencephalopathy; CHX, cycloheximide; CLC, chloride channel; MLC, megalencephalic leukoencephalopathy with subcortical cysts; NSFA, non-stationary fluctuation analysis; PM, plasma membrane; WT, wild-type.

Introduction

ClC-2 is a ubiquitously expressed chloride channel that belongs to the family of CLC channel/transport proteins (Jentsch, 2015). Early insight into its physiological role came from studies using *Clcn2* knockout mice, which revealed that ClC-2 protein depletion caused male germ cell and photoreceptor degeneration, possibly through disruption of the ionic environment where these cells occur (Bosl *et al.* 2001). Subsequent studies showed that these knockout mice also developed vacuolisation in the brain (Blanz *et al.* 2007). Electron microscopic analysis of *Clcn2* knockout mice revealed that the vacuoles were present within the myelin, similar to that observed in humans affected by a rare form of leukodystrophy called megalencephalic leukoencephalopathy with subcortical cysts (MLC; OMIM no. 604004) (van der Knaap *et al.* 2012), thereby suggesting that *CLCN2* mutations might cause MLC. However, *CLCN2* mutations were not found in MLC patients lacking *MLC1* mutations (the most frequent cause of the disease) (Leegwater *et al.* 2001) and, subsequently, its role in MLC was discarded (Scheper *et al.* 2010).

More recent studies, however, have identified *CLCN2* mutations in patients suffering from a type of leukodystrophy (OMIM no. 615651; *CLCN2*-related leukoencephalopathy (CC2L); Depienne *et al.* 2013). These patients show intramyelinic oedema of specific brain structures, such as the posterior limbs of the internal capsules, cerebral peduncles in the midbrain, pyramidal tracts in the pons and middle cerebellar peduncles (Depienne *et al.* 2013). Clinical manifestations of the disease are variable and may include cerebellar ataxia, spasticity, optic neuropathy and chorioretinopathy with visual field defects (Depienne *et al.* 2013). Furthermore, two patients with *CLCN2* mutations were described as showing additional clinical manifestations, such as infertility (Di Bella *et al.* 2014) and secondary paroxysmal kinesigenic dyskinesia (Hanagasi *et al.* 2015). Recently, new patients with mutations in *CLCN2* have been identified expanding the spectrum of mutations identified (Giorgio *et al.* 2017; Zeydan *et al.* 2017). Given that some of these phenotypes have been observed in *Clcn2* knockout mice (Bosl *et al.* 2001; Blanz *et al.* 2007), these animals can be used to further our understanding of the molecular basis of *CLCN2*-related leukodystrophy (CC2L).

Several *CLCN2* mutations have been identified in CC2L patients, with some of the insertion or deletion mutations leading to the total loss of the ClC-2 protein (Depienne *et al.* 2013). A missense mutation (Ala500Val, A500V) and an in-frame deletion of two amino acids (Leu144_Ile145del, L144_I145del) were the first mutations identified in leukodystrophy patients (Fig. 1), both mutations considerably decreasing the plasma membrane (PM) expression of ClC-2 in COS-7 cells (Depienne *et al.* 2013). It is still unknown whether these mutations also affect channel activity. New mutations have been recently identified in other CC2L patients (van der Knaap *et al.* 1993), but no detailed biochemical or functional investigations have been performed to date.

The cell adhesion protein GlialCAM regulates the activity and localisation of ClC-2 in glial cells (Jeworutzki *et al.* 2012). *GLIALCAM* was originally identified as the second gene involved in MLC pathogenesis (Lopez-Hernandez *et al.* 2011*a*,*b*), *MLC1* being the first (Leegwater *et al.* 2001). GlialCAM is part of the MLC1 macromolecular complex. It acts as a chaperone for MLC1 and targets it to cell–cell junctions (Capdevila-Nortes *et al.* 2013). In addition, GlialCAM restricts ClC-2 localisation to cell–cell junctions and modulates ClC-2 channel activity (Barrallo-Gimeno & Estévez, 2014; Barrallo-Gimeno *et al.* 2015). The latter is accomplished by increasing current amplitudes of ClC-2, as well as changing the rectification and activation properties of the channel by affecting its common gating (Jeworutzki *et al.* 2014). Since ClC-2 can reach the PM independently of GlialCAM and as the cell surface density of ClC-2 remains largely unaltered upon co-expression with GlialCAM (Jeworutzki *et al.* 2012), GlialCAM was originally considered a subunit modulating ClC-2 function. However, the observation that loss of GlialCAM or MLC1 reduces ClC-2 protein expression in the cerebellum (Hoegg-Beiler *et al.* 2014) suggests that GlialCAM and MLC1 may contribute to ClC-2 stabilisation through unknown mechanisms. Furthermore, recent results have indicated that ClC-2 may form a ternary complex with GlialCAM and MLC1 in astrocytes (Sirisi *et al.* 2017). It is currently unknown whether GlialCAM and MLC1 have a role in stabilising ClC-2.

In the present study, we analysed the biochemical and functional consequences of most *CLCN2* missense mutations that have been identified in patients with leukodystrophy. The role of GlialCAM and MLC1 on the functional expression of ClC-2 was also investigated.

Methods

Ethics

All the animal experimental protocols were approved by the Animal Care and Ethics Committee of the University of Barcelona and approved by the Government of Catalonia. All animal protocols conformed to the European Community Guidelines on Animal Care and Experimentation.

Molecular biology

Plasmids were constructed using standard molecular biology techniques employing recombinant PCR and the Multisite Gateway System (Thermo Fisher Scientific, Waltham, MA, USA). All cloned constructs were checked by sequencing. Human ClC-2 with an extracellular haemagglutinin (HA) tag (provided by Pablo Cid, Centro de Estudios Científicos, Chile) and human GlialCAM with a FLAG-tag at the C-terminus (3 FLAG copies) were used.

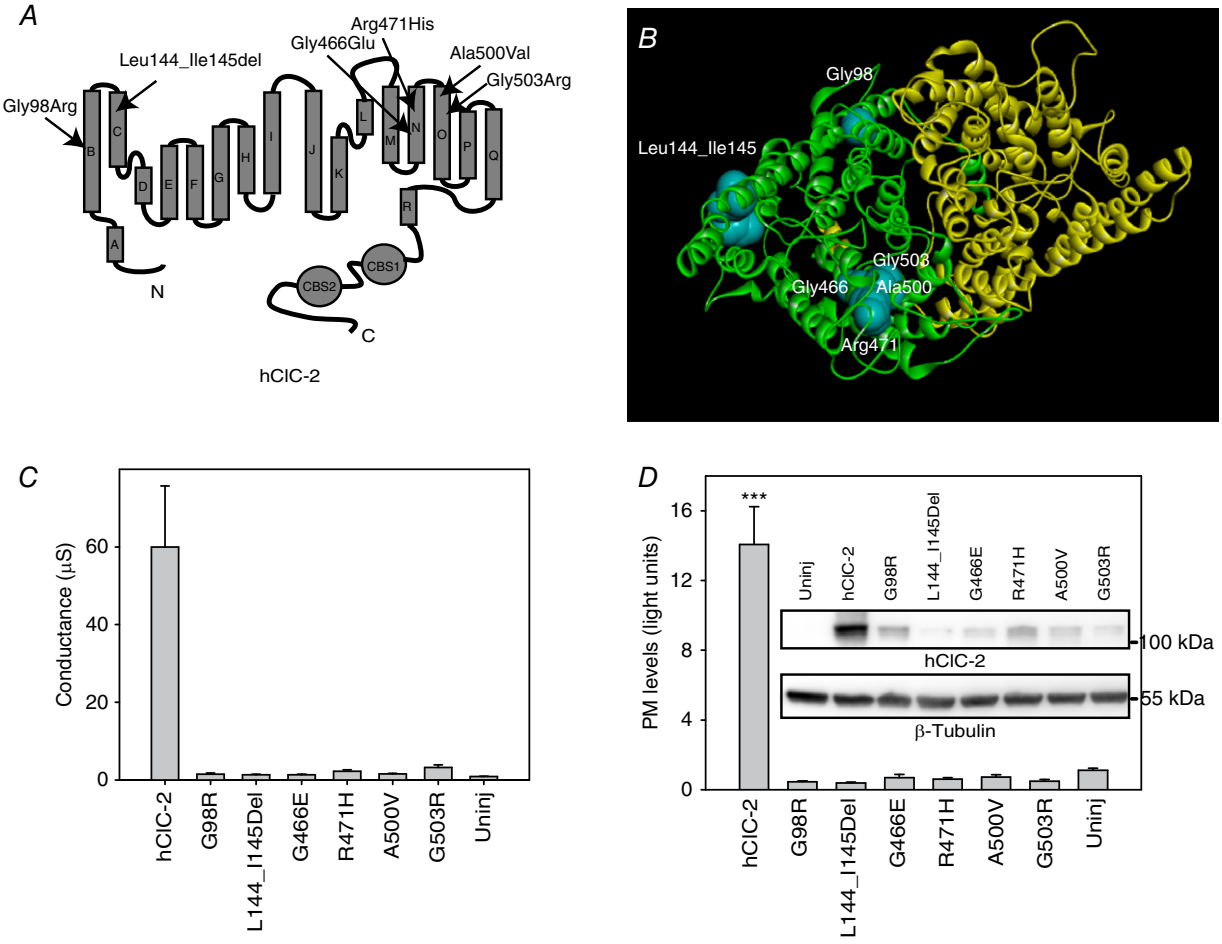

Figure 1. Functional expression of ClC-2 mutants in *Xenopus* oocytes
A, schematic 2-D model of the ClC-2 chloride channel. The estimated positions of several *CLCN2* mutations identified in leukodystrophy patients are indicated. The localisation of the N- and C-terminus is shown. The helices and the position of the cystathionine β-synthase (CBS) domains of the ClC-2 protein are also shown. *B*, 3-D model of the TM domains of human ClC-2 obtained using the automated Swissprot homology modelling service (Biasini *et al*. 2014). Each of the monomers is indicated by a different colour. The amino acids that are mutated in leukodystrophy are shown as CPK models with one of the monomers in blue. *C*, conductance values mediated by human wild-type (WT) ClC-2 or ClC-2 containing the indicated mutation. Uninj, uninjected oocytes. Data represent the mean ± SEM ($n = 5$ for all the groups). ***$P < 0.001$ (Student's *t* test comparing the mutant with WT ClC-2). Two additional experiments gave similar results. *D*, chemiluminescence assay for cell PM expression shows a reduced expression of ClC-2 mutants compared to WT ClC-2 (uninjected oocytes, $n = 10$; hClC-2, $n = 10$; G98R, $n = 15$; L144_I145del, $n = 10$; G466E, $n = 18$; R471H, $n = 18$; A500V, $n = 11$; and G503R, $n = 10$). Another independent experiment gave similar results. PM, plasma membrane. ***$P < 0.001$ compared to the human WT ClC-2 (hClC-2) (Student's *t* test). Inset: western blot analysis using the same oocytes showing that the steady-state levels of the ClC-2 protein are reduced for all mutations. β-Tubulin was used as the loading control. Another independent experiment gave similar results. [Colour figure can be viewed at wileyonlinelibrary.com]

For some patch clamp studies (non-stationary fluctuation analysis (NSFA)), we used rat ClC-2, which was fused to green fluorescent protein (GFP) at its C-terminus. The fusion of GFP to the C-terminus of ClC-2 does not affect channel activity (Jeworutzki *et al.* 2012). For fluorescence assays using SNAP-Cell® TMR-Star (New England Biolabs, Ipswich, MA, USA), human ClC-2 was fused to a SNAP-tag at its C-terminus. We used human wild-type (WT) and mutant R92W GlialCAM with a FLAG-tag at the C-terminus (3 FLAG copies).

Primary culture and adenoviral transduction

Rat quiescent primary astrocyte cultures were prepared from P0–P2 pups, as described previously (Duarri *et al.* 2011). Briefly, postnatal pups of both sexes were killed by rapid decapitation; their cortex and hippocampus were aseptically removed from newborn (1–3 days old) Sprague–Dawley rats (Charles River, Barcelona, Spain). Cerebral cortices were dissected and the meninges were carefully removed in cold sterile 0.3% BSA and 0.6% glucose in PBS. The tissue was trypsinised for 10 min at 37°C and mechanically dissociated in complete Dulbecco's modified Eagle's medium (DMEM; with 10% heat-inactivated fetal bovine serum (Biological Industries, Kibbutz Beit Haemek, Israel), 1% penicillin/streptomycin (Thermo Fisher Scientific) and 1% glutamine (Thermo Fisher Scientific) plus 40 U ml^{-1} DNase I (Sigma-Aldrich, St Louis, MO, USA)) through a small bore fire-polished Pasteur pipette. The cell suspension was pelleted and resuspended in fresh complete DMEM, filtered through a 100 μm nylon membrane (BD Falcon, Corning, Pozuelo de Alarcon, Madrid, Spain) and plated into 75 cm^2 cell-culture flasks (TPP, Sigma-Aldrich). When the mixed glial cells reached confluence, contaminating microglia, oligodendrocytes and precursor cells were dislodged by mechanical agitation. Astrocytes were plated in six-well plates at a density of 4×10^5 cells per well or in poly-D-lysine-coated coverslips at 7.5×10^4 cells per 24-well plate. Medium was changed every 3 days. To increase the expression of MLC1 and GlialCAM detection at the plasma membrane (data not shown), we arrested astrocytic cultures in the cell cycle by addition of 2 μM cytosine β-D-arabinofuranoside (AraC, Sigma-Aldrich). Cultured astrocytes were identified by their positive glial fibrillary acidic protein staining (Dako, Carpenteria, CA, USA).

Adenoviruses expressing human GlialCAM with three copies of the FLAG epitope fused to the C-terminus were constructed, as described before (Lopez-Hernandez *et al.* 2011*a*). Similarly, adenoviruses expressing HA-tagged WT or mutant ClC-2 (containing the mutation A500V) were also constructed. Transduction of astrocytes with the adenovirus construct was performed as previously described (Duarri *et al.* 2008).

RNA interference in HeLa cells

To knock down endogenous GlialCAM expression in HeLa cells, lentiviral vectors (pGIPZ) for the constitutive expression of microRNA-adapted short hairpin RNA (shRNAmir) specific for GlialCAM (GIPZ, V2LMM_69402 and V3LHS_413353) and a non-targeted variant (NT, ATCTCGCTTGGGCGAGAGTAAG) were obtained from Thermo Fisher Scientific–Open Biosystems (USA). Lentiviruses were produced and HeLa cells transduced, as described before (Capdevila-Nortes *et al.* 2013).

Transfection, immunofluorescence and plasma membrane surface analysis in transfected cells by cell surface ELISA or cell surface biotinylation

HeLa cells were grown in DMEM containing 10% (v/v) fetal bovine serum (FBS; Sigma-Aldrich), 1% glutamine and 1% penicillin/streptomycin at 37°C in a humidity controlled incubator with 5% CO_2. Cells were transfected with the TransFectin™ Lipid Reagent (Bio-Rad, Hercules, CA, USA). Twenty-four hours after transfection, cells were transferred to glass-covered Petri dishes for experiments that were performed after another 24–48 h. To study ClC-2 and GlialCAM localisation, cells were fixed and processed as previously described (Jeworutzki *et al.* 2012). The following antibodies were used: anti-FLAG (diluted 1:500) and anti-ClC-2 (diluted 1:100) antibodies (Jeworutzki *et al.* 2012). For western blot studies, cell lysates were prepared and processed as previously described (Capdevila-Nortes *et al.* 2013), with β-actin protein levels used as the loading control. For densitometric analysis of proteins on western blots, at least three western blots were obtained for each type of analysis. Scanned images were quantified for the densitometric analysis using ImageJ (http://rsbweb.nih.gov/ij/).

PM density of ClC-2 and the efficiency of GlialCAM knockdown were determined by cell surface ELISA, as described previously in HeLa cells (Capdevila-Nortes *et al.* 2013). Briefly, HeLa cells expressing shGlialCAM (Capdevila-Nortes *et al.* 2013) were transfected with ClC-2 cDNA constructs using Lipofectamine® 2000 (Thermo Fisher Scientific) 48 h prior to analysis. The extracellular epitope was detected with mouse anti-human HepaCAM (1:1000, R&D Systems, Minneapolis, MN, USA) and mouse anti-HA (1:1,000, cl11, Covance, Sherwood Park, AB, Canada) primary antibodies, and horseradish peroxidase (HRP)-conjugated secondary F(ab′)2 antibody (Jackson ImmunoResearch Laboratories, West Grove, PA, USA) together with Amplex®Red fluorogenic substrate (Thermo Fisher Scientific). The fluorescence signal was measured using an Infinite® M1000 fluorescence plate reader (Tecan Group Ltd, Männedorf, Switzerland), with an excitation and emission wavelength of 544 nm and 590 nm, respectively. IgG isotype control (Sigma-Aldrich)

served to determine non-specific antibody binding. ClC-2 internalisation and stability were calculated from the loss of the initially labelled ClC-2 PM pool after a chase period, and expressed as a percentage of the initial ClC-2 density.

To detect ClC-2 surface levels, HeLa or HEK293T cells were cultured in 10 cm plates. They were washed three times with PBS with 1 mM $CaCl_2$ and 1 mM $MgCl_2$ (PBS-CM). Subsequently, cells were incubated on ice for 30 min in PBS-CM containing 3 mg ml^{-1} EZ-Link™ Sulfo-NHS-Biotin (Thermo Fisher Scientific). After three washes with PBS-CM, they were quenched for 10 min in PBS Ca/Mg containing 10 mM lysine. After three additional washes with PBS-CM, cells were lysed for 1 h in RIPA buffer (50 mM Tris pH 8, 150 mM NaCl, 1% NP-40, 0.5% deoxycholate, 0.1% SDS, 2 mM EDTA) containing protease inhibitors. After centrifugation for 15 min at 18400 g, the lysate was quantified using the BCA protein assay (Thermo Fisher Scientific). One milligram of the solubilised extract in a total volume of 200 μl was incubated with 100 μl of streptavidin agarose (Thermo Fisher Scientific) O/N at 4°C. After a brief centrifugation, the supernatant (SN) was taken and beads were washed three times with RIPA buffer. Biotinylated proteins were eluted with Load sample buffer (LSB) 1× for 15 min at 65°C. Samples of lysate, supernatant and eluate were analysed by western blot. To confirm that only surface membrane proteins were present in the eluate, we performed a western blot with antibodies detecting the endoplasmic reticulum resident protein calnexin.

Electrophysiology and luminescence-based surface assays in *Xenopus* oocytes

Oocytes were obtained by surgery from *Xenopus laevis* purchased from Xenopus Express (Vernassal, France). Oocytes were harvested from frogs that had been anaesthetised by Tricaine (ethyl 3-aminobenzoate methanesulfonate salt; Sigma-Aldrich) and the follicular layer was enzymatically removed as described by Estevez *et al.* (2003). After surgery, frogs were allowed to recover from anaesthesia and suitable aftercare was given. Oocytes were kept at 17°C in Barth's solution containing, in mM: 88 NaCl, 1 KCl, 0.82 $MgSO_4$, 0.41 $CaCl_2$, 0.33 $Ca(NO_3)_2$, 2.4 $NaHCO_3$ and 10 HEPES/Tris, pH 7.4, as well as 10 mg l^{-1} of gentamycin. Each oocyte was injected with 10 ng of capped ClC-2 complementary RNA (cRNA). To analyse the ClC-2/GlialCAM complex, 1.25 ng of GlialCAM cRNA was co-injected with ClC-2. Measurements were carried out in ND96 medium (96 mM NaCl, 2 mM KCl, 1.8 mM $CaCl_2$, 1 mM $MgCl_2$ and 5 mM HEPES buffer at pH 7.4). For pH experiments, HEPES was replaced with 5 mM MES buffer (pH 5.4 and 6.4) and 5 mM Tris buffer (pH 8.4). The voltage protocol involved an initial 100 ms voltage pulse at −30 mV, followed by 4 s voltage steps from +80 to −140 mV in 20 mV increments, and a tail pulse of 1 s at +40 mV, followed by another 100 ms pulse at −30 mV. Currents were measured using a TEC-05X voltage amplifier and the CellWorks© program (NPI Electronic, Tamm, Germany). Off-line analysis was performed using pCLAMP9 (Molecular Devices, Sunnyvale, CA, USA) and SigmaPlot (Systat Software, Inc., San Jose, CA, USA).

To measure surface membrane expression of mutant and WT channels, we used HA-tagged ClC-2 constructs (Cornejo *et al.* 2009) and a chemiluminescence-based technique as described earlier (Duarri *et al.* 2008). Briefly, oocytes were placed in ND96 medium containing 1% BSA for 30 min at 4°C, then incubated for 60 min at 4°C with 1 μg ml^{-1} of rat monoclonal anti-HA antibody (3F10, Roche Diagnostics, Sant Cugat del Vallès, Barcelona) in 1% BSA–ND96, before being washed at 4°C and incubated with HRP-conjugated secondary antibody (donkey anti-rat IgG (H+L); Jackson ImmunoResearch, Newmarket, UK) in 1% BSA–ND96 for 30–60 min at 4°C. Oocytes were washed thoroughly (1% BSA at 4°C for 60 min) and transferred to ND96 without BSA. Individual oocytes were placed in 50 μl of Power Signal ELISA solution (Thermo Fisher Scientific). Chemiluminescence was quantified in a Turner TD-20/20 luminometer (Turner BioSystems, Sunnyvale, CA, USA).

Fluorescence labelling with SNAP-Cell® TMR-Star and microscopic analysis

HeLa cells transfected with the different SNAP-tag-containing ClC-2 constructs with or without GlialCAM were pulse-labelled with SNAP-Cell® TMR-Star (3 mM) dissolved in DMEM for 15 min at 37°C. The cells were washed three times with the culture medium and incubated for another 30 min at 37°C. For microscopic analysis at different time points, cells were fixed with 3% paraformaldehyde for 15 min at room temperature and washed with PBS. To detect GlialCAM, the FLAG epitope fused to GlialCAM was analysed by immunofluorescence. Images were taken on an Olympus DSU confocal microscope using an EM-CCD camera (Hamamatsu, Cerdanyola, Barcelona, Spain). The settings of the camera (acquisition time and EM gain) were manually adjusted for each experimental group to give sufficient sensitivity and prevent saturation. The fluorescence of the SNAP-Cell® TMR-Star was measured at short exposure times (to avoid saturation) using the same exposure times for each group. To quantify the fluorescence signal, the area of interest of each cell was manually selected and the average grey value measured using ImageJ. The average grey value of the background was subtracted from the average grey value of the area of interest for each image.

Patch-clamp experiments in HEK293T cells

HEK293T cells were cultured in DMEM containing 10% FBS, 1% penicillin/streptomycin and 1% L-glutamine.

Cells were transiently transfected for 24 h with ClC-2-GFP or A500V-ClC-2-GFP alone or with GlialCAM using FuGENE® transfection reagent (Roche), following the manufacturer's instructions. Electrophysiological recordings were performed with a patch-clamp amplifier (Axopatch 200B, Molecular Devices). Patch electrodes were fabricated in a Flaming–Brown micropipette puller P-97 (Sutter Instrument Co., Novato, CA, USA). Electrodes had a resistance of 3–5 MΩ when filled with an intracellular solution containing (in mM): 130 NaCl, 2 $MgSO_4$, 2 EGTA and 10 HEPES/NaOH, pH 7.3, at an osmolality of 304 ± 2 mosmol kg^{-1}. The extracellular solution contained (in mM): 140 NaCl, 2 $MgSO_4$, 2 $CaCl_2$ and 10 HEPES/NaOH, pH 7.3, at an osmolality of 308 ± 3 mosmol kg^{-1}. All solution osmolalities were adjusted with sorbitol. An Ag–AgCl ground electrode mounted in an agar bridge of 3 M KCl was used. Membrane currents were recorded in the whole-cell patch clamp configuration, filtered at 2 kHz, digitised at 10 kHz and acquired with pCLAMP10 software (Molecular Devices). Data were analysed with Clampfit 10 (Molecular Devices) and Prism 4 (GraphPad Software, Inc., La Jolla, CA, USA). Whole-cell capacitance and series resistance were compensated with the amplifier circuitry. Series resistance was always kept below 10 MΩ and compensated at 70–80%. All recordings were performed at room temperature (22–23°C). Currents were evoked with 3 s pulses from +60 to −140 mV from a holding potential of 0 mV.

Single-channel conductance estimates were determined in transfected HEK293T cells in the whole-cell configuration from currents activated at −100 mV and tail currents at +60 mV by using NSFA, as previously described for ClC channels (Pusch *et al.* 1994; Jeworutzki *et al.* 2012). Briefly, the ensemble variance of all successive pairs of current responses was calculated to infer channel properties from macroscopic responses. The single-channel current (i) was determined by plotting this ensemble variance (σ^2) against mean current (I) and fitting this to a parabolic function:

$$\sigma^2 = \sigma_B^2 + \left(i\bar{I} - \left(\frac{\bar{I}^2}{N}\right)\right)$$

where $\sigma_B{}^2$ denotes the background variance and N the number of channels contributing to the response. The mean response was calculated from recordings containing 25–40 stable responses, which were identified by a Spearman's rank-order correlation test (using Igor Pro with NeuroMatic software). The weighted mean single-channel conductance was calculated from the single-channel current at the holding potential of +60 mV ($\gamma = i/V_{hold}$) from the deactivating phase due to the slow activating kinetics of A500V-ClC-2, which make the NSFA of the mutant at the holding potential of −100 mV problematic mainly for the low range of current levels available for analysis.

As seen in Fig. 3, the experimental data used in the NSFA cover only part of the best least square parabola fitted to the mean–variance experimental points that calculate single-channel currents. Nevertheless, unitary current estimates from such an analysis have been shown to be reliable and do not differ greatly from fittings in ideal conditions where variance data cover the whole range of the mean current (Alvarez *et al.* 2002). To assess if leak current could affect the NSFA measurement, iodide replacement or cadmium addition (0.2 mM) was used to inhibit ClC-2 current and to estimate the amount of leak current. The measured leak current was subtracted and NSFA performed as described. No significant differences were found between the single-channel conductance estimated in leak-subtracted and non-subtracted experiments.

Statistics

Values correspond to means ± SEM. Student's unpaired t test was used to determine statistical significance between groups. $^{*}P < 0.05$; $^{**}P < 0.01$; $^{***}P < 0.001$.

Results

Electrophysiological characterisation of ClC-2 mutants in *Xenopus* oocytes

We first investigated the functional effect of most *CLCN2* mutations identified in patients with leukodystrophy (van der Knaap *et al.* 1993), which are predicted to occur in the transmembrane (TM) helices B (G98R), C (L144_I145del), N (G466E and R471H) and O (A500V and G503R) (Fig. 1*A*). Interestingly, some of the mutations cluster in the same region, while none are found in the contact regions of the homodimer (Fig. 1*B*), consistent with the recessive character of the mutations. We engineered ClC-2 variants by PCR mutagenesis, using the human wild-type (WT) channel bearing an HA loop connecting the L and M TM helices. The HA-tag does not interfere with ClC-2 function, as shown previously (Cornejo *et al.* 2009). The cRNAs of ClC-2 variants were injected into *Xenopus* oocytes and membrane currents measured by two-electrode voltage clamp, as previously described (Jeworutzki *et al.* 2012). Expression of human ClC-2 in oocytes elicited a slowly activated chloride current upon hyperpolarisation (Pérez-Rius *et al.* 2014) (Fig. 1*C*). By contrast, none of the ClC-2 variants produced significantly higher currents than those measured in uninjected oocytes (Fig. 1*C*).

To determine whether compromised channel expression and/or function contributes to the loss-of-function phenotype of the ClC-2 mutants, the expression

levels and PM density of the ClC-2 mutants were compared by western blotting and luminescence-based cell surface ELISA, respectively. All mutants showed reduced protein expression (Fig. 1*D*, inset), and PM expression was similar for injected and uninjected oocytes based on their comparable luminescence signal (Fig. 1*D*), suggesting that the defective functional expression of ClC-2 mutants can be attributed, at least partly, to their severely impaired total and PM expression.

Functional and biochemical analyses of ClC-2 mutants in mammalian cells

We focused on characterising the A500V mutation, which was the first identified in CC2L patients (van der Knaap *et al.* 1993). To elucidate the underlying mechanism of the loss-of-function phenotype of ClC-2 mutations in mammalian cells, whole-cell patch-clamp analysis was performed in HEK293T cells transiently expressing WT ClC-2 or A500V-ClC-2. WT ClC-2 expression generated a mean maximum current of -182.1 ± 31.3 pA pF^{-1} ($n = 17$) at -140 mV (Fig. 2*B* and *D*) compared to untransfected cells (-0.8 ± 0.4 pA pF^{-1}; $n = 6$) (Fig. 2*A*). By contrast, A500V-ClC-2 elicited a much more reduced current by about 13-fold (-12.2 ± 6.5 pA pF^{-1}; $n = 9$) (Fig. 2*C* and *D*; note the different current scales) compared to WT ClC-2 in HEK293T cells.

A500V-ClC-2 exhibited accelerated deactivation kinetics, based on the comparison of tail currents at +60 mV (Fig. 2*B* and *C*). The mutant deactivation kinetics ($\tau = 92.2 \pm 25.7$ ms; $n = 9$) was significantly faster when compared to WT ClC-2 ($\tau = 348.8 \pm 101.1$ ms; $n = 17$; $P < 0.05$), indicating that the A500V mutation impairs channel gating. Importantly, currents observed in A500V-ClC-2 cells were blocked by iodide and the mutant was expressed at the PM in HEK293T cells (measured by surface biotinylation, data not shown), indicating that these currents were mediated by the expressed protein and not due to endogenous channels.

The effect of the A500V mutation on ClC-2 expression was determined by immunoblotting transfected HeLa cells. The mutation reduced ClC-2 expression to about 20% of that of WT ClC-2 expression (Fig. 2*E*). The significant decrease could be attributed partly to the compromised stability of the mutant channels, as indicated by the disappearance kinetics of the cellular ClC-2 pool using cycloheximide (CHX) chase analysis and immunoblotting (Fig. 2*F*). It should be noted that the blot of the mutant channel was overexposed to better visualise the decrease in expression. A500V-ClC-2 displayed significantly reduced stability compared to WT ClC-2 (Fig. 2*F*). Unexpectedly and in contrast to the results from the *Xenopus* oocytes, PM ELISA revealed that the mutation only produced a 50% reduction in the PM density of the mutant ClC-2 compared to WT ClC-2 (Fig. 2*G*). To estimate surface expression by an alternative method, we performed surface biotinylation assays using sulpho-NHS-biotin (Fig. 2*H*). From three independent experiments, the mutant A500V-ClC-2 has an expression level about 12% of that of WT ClC-2 at the PM (Fig. 2*H*). Thus, we conclude that the mutant has a reduced surface expression compared to the WT channel, although the percentage of reduction differs between the experimental methods used for analysis.

A500V-ClC-2 does not have altered single-channel conductance

The A500V mutation may attenuate ClC-2-mediated Cl^- currents by several mechanisms. It can decrease the number of channels (N) at the PM, open probability (P_{open}) or single-channel conductance (γ), individually or in combination, at a given electromotive force ($V - V_{equilibrium}$), based on the equation that defines the magnitude of the macroscopic current (I) for any given channel ($I = N \times P_{open} \times \gamma \times (V - V_{equilibrium})$). Our results indicate that the number of channels at the PM is reduced by approximately 50% (Fig. 2*G*), whereas the macroscopic current is decreased by about 95% (Fig. 2*D*), consistent with a severe defect in gating and/or conductance.

We used NSFA to evaluate a possible reduction in the unitary conductance of A500V-ClC-2 (γ). As human ClC-2 generates a smaller current than rat ClC-2, we decided to perform this analysis with rat ClC-2. Furthermore, this analysis has been performed already with rat ClC-2 (Jeworutzki *et al.* 2012), thus enabling easy comparison. We introduced an analogous mutation of A500V into the rat ClC-2 orthologue, as the A500 residue is conserved between the human and rat channels. The mutation significantly reduced the current amplitudes of the rat ClC-2. The mean maximum current mediated by the rat WT ClC-2 and A500V-ClC-2 at -140 mV was -272.4 ± 35.4 pA pF^{-1} ($n = 9$) and -13.5 ± 5.1 pA pF^{-1} ($n = 9$), respectively. To test whether the A500V mutation affected single-channel conductance of the rat ClC-2, we performed NSFA using tail deactivating currents at a holding voltage of +60mV (Fig. 3*A*–*D*). Since the detection of current was more reliable at +60 mV for the mutant, we validated this approach by comparing the single-channel conductance for rat WT ClC-2 obtained by tail current measurements at +60 and -100 mV voltage steps (see 'Methods' for additional details). There was no significant difference between the two voltage steps (3.02 ± 0.55 *vs.* 2.99 ± 0.46 pS measured at -100 and +60 mV, respectively; $P = 0.975$; $n = 12$). Our results were very similar to those obtained by Jeworutzki *et al.* (2012) for the rat ClC-2. There was no significant difference between the conductance of rat WT ClC-2 and that of A500V-ClC-2 (2.99 ± 0.46 pS for WT ClC-2 *vs.*

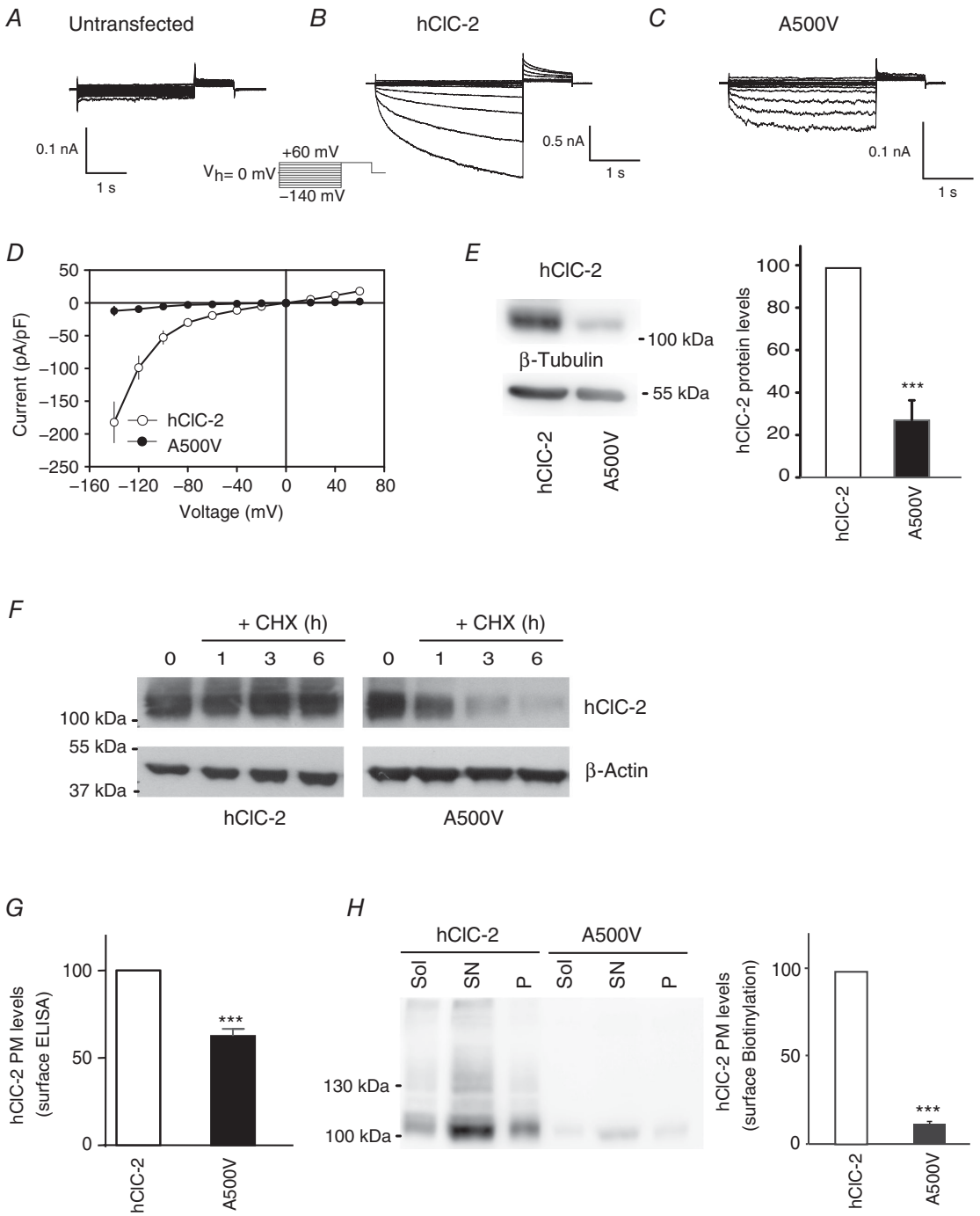

Figure 2. Biochemical and functional analyses of ClC-2 mutants in cell lines
A–C, typical current traces obtained in (*A*) untransfected HEK293T cells, (*B*) cells transfected with human WT ClC-2 and (*C*) cells transfected with human A500V-ClC-2. Starting from a holding potential of 0 mV, voltage pulses were applied from +60 mV to −140 mV in 20 mV increments, followed by a pulse at 60 mV before finally returning to 0 mV, as indicated in the inset in *A*. The scale used is shown in each group. *D*, steady-state current–voltage relationship of human WT ClC-2 ($n = 17$; open circles) and human A500V-ClC-2 ($n = 9$; filled circles). *E*, total cellular ClC-2 protein expression. HeLa cells were transfected with the indicated ClC-2 plasmids. Forty-eight hours later, extracts were analysed by western blotting. β-Actin was used as the loading control. Quantification of the proteins on the blots from eight independent experiments was performed using ImageJ. The value for WT ClC-2 was normalised to 100%. Student's *t* test was used to compare the expression levels of A500V-ClC-2 and WT ClC-2: $^{***}P < 0.001$. *F*, decreased total protein stability of A500V-ClC-2. HeLa cells transfected with the indicated ClC-2 plasmids were incubated with the protein synthesis inhibitor CHX (100 μg ml^{-1}) for the indicated times (0, 1, 3 and 6 h). Cells were harvested, solubilised and analysed by western blotting. A representative western blot

from four independent experiments is shown. The blots containing A500V-ClC-2 were overexposed to visualise the decrease in protein expression. *G*, PM expression of human WT ClC-2 and A500V-ClC-2 was determined by cell surface ELISA in HeLa cells. Data were normalised to that of the WT ClC-2. ***$P < 0.001$ (Student's *t* test). PM, plasma membrane. *H*, HeLa cells expressing human WT ClC-2 and A500V-ClC-2 were biotinylated, solubilized and affinity purified using streptavidin as detailed in 'Methods'. Aliquots of the solubilized extract (Sol), the supernantant of the purification (SN) and the purification (P) were processed by western blot using the 3F10 antibody. A representative experiment is shown. Blots were overexposed to visualize the low levels of protein present in the pellet. Quantification of the levels found in the purified sample (biotinylated proteins in the membrane) from three different experiments revealed that the levels of A500V-ClC-2 in the membrane were about 12% of that of WT ClC-2 at the PM. Data were normalised to that of the WT ClC-2. ***$P < 0.001$ (Student's *t* test).

3.45 ± 0.79 pS for A500V-ClC-2; $P = 0.728$; $n = 12$ and 8, respectively; Fig. 3*D*).

Taken together, our results indicate that the defective functional expression of A500V-ClC-2 results from a complex mechanism involving reduced PM density and stability, as well as impaired gating.

Functional modulation of ClC-2 mutants by GlialCAM

Jeworutzki *et al.* (2012) observed that the co-expression of WT ClC-2 with GlialCAM in *Xenopus* oocytes dramatically increased the amplitude of chloride currents (Fig. 4*A* and *C*). In the present study, GlialCAM changed the rectification properties of ClC-2, which conducted at positive voltages in the presence of GlialCAM, and increased the activation kinetics of the channel, which displayed an instantaneous opening (compare Figs 4*A* and 2*B*). Surprisingly, GlialCAM partially rescued A500V-ClC-2 function in oocytes (Fig. 4*B* and *C*). These currents were blocked by iodide, indicating that the mutant A500V together with GlialCAM retained the ion channel selectivity of CLC proteins and the currents observed were not due to other channels present in the *Xenopus* oocyte system.

GlialCAM has been reported to increase ClC-2 current by changing the common gate of the channel (Jeworutzki *et al.* 2014), the lack of inhibition of the current at acidic pH being linked to an increased activation of the common gate (Zuniga *et al.* 2004; Jeworutzki *et al.* 2012). Thus, the activity of human A500V-ClC-2 was not inhibited at

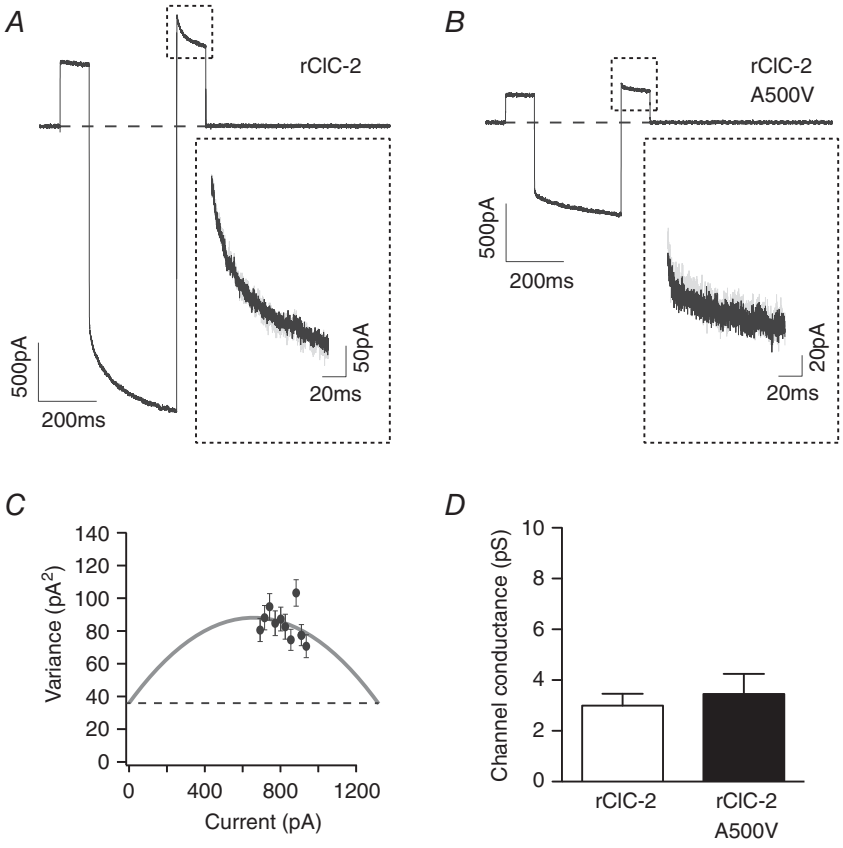

Figure 3. Fluctuation analysis of the single-channel conductance of rat ClC-2 containing the A500V mutation
A and *B*, representative recordings for rat WT ClC-2 (*A*) and A500V-ClC-2 mutant channel (*B*). From a holding voltage of 0 mV, membrane voltage was stepped to +60, −100 and +60 mV. Tail currents from the second pulse at +60 mV were used for non-stationary fluctuation analysis (magnified in the inset). The average trace is shown in black, while a single sweep is shown in grey. *C*, current variance *vs.* mean current for the recording shown in *A*. *D*, mean single-channel conductance (pS) for WT ClC-2 ($n = 12$) and A500V-ClC-2 ($n = 8$). No significant differences were found between the WT and mutant channels ($P = 0.7285$, Mann–Whitney *U* test).

acidic pH when co-expressed with GlialCAM in *Xenopus* oocytes, but it was inhibited when expressed alone (Fig. 4*D*). Based on these results, GlialCAM might stimulate the A500V-ClC-2 current by modifying its gating properties.

Co-expression with GlialCAM also increased the currents mediated by rat WT ClC-2 (Fig. 4*E* and *G*) and A500V-ClC-2 in HEK293T cells (Fig. 4*F* and *G*). Since GlialCAM co-expression does not affect the single-channel conductance of rat WT ClC-2 (Jeworutzki *et al.* 2012),

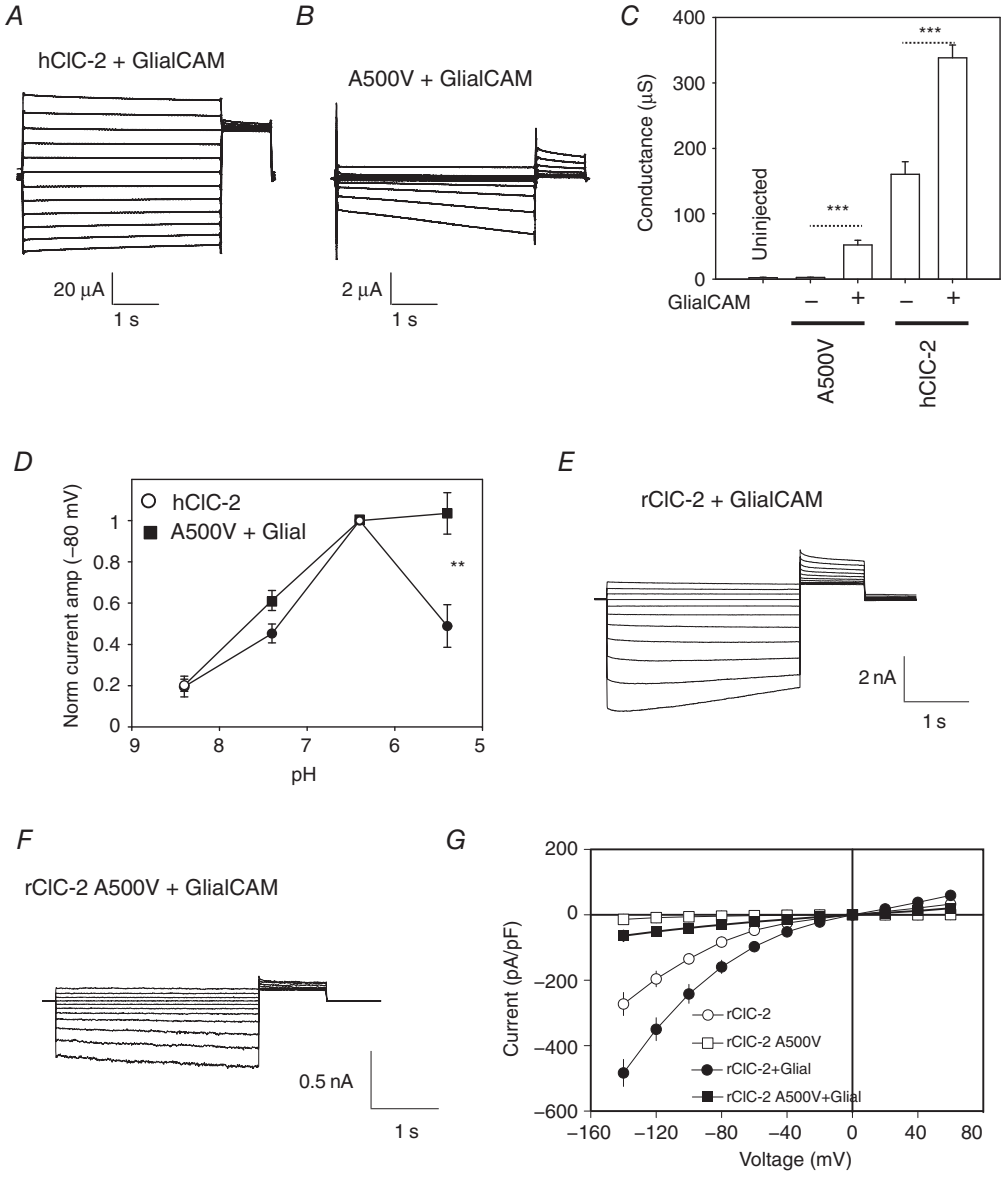

Figure 4. Functional effect of GlialCAM on ClC-2 mutants expressed in *Xenopus* oocytes and HEK293T cells

A and *B*, typical current traces of (*A*) human WT ClC-2 + GlialCAM and (*B*) human A500V-ClC-2 + GlialCAM. The scale is shown for each experimental group. *C*, conductance values (in μS) were measured by analysing steady-state current–voltage relationships. Uninjected oocytes, $n = 9$; oocytes injected with A500V-ClC-2, $n = 22$; oocytes injected with A500V-ClC-2 + GlialCAM, $n = 27$; oocytes injected with WT ClC-2, $n = 7$; and oocytes injected with WT ClC-2 + GlialCAM, $n = 4$. $^{***}P < 0.001$ compared to oocytes without GlialCAM (Student's *t* test). *D*, pH dependence of human WT ClC-2 (open circles, $n = 4$) and A500V-ClC-2 + human GlialCAM (filled squares, $n = 7$). Currents were normalised to the value at pH 6.4 for each experimental group. $^{**}P < 0.01$ compared to human WT ClC-2 alone (Student's *t* test). *E* and *F*, typical current traces obtained in cells transfected with rat ClC-2 plus GlialCAM (*E*) and cells transfected with rat A500V-ClC-2 plus GlialCAM (*F*). *G*, steady-state current–voltage relationship of rat WT ClC-2 ($n = 9$; open circles), rat WT ClC-2 + GlialCAM ($n = 6$; filled circles), rat A500V-ClC-2 ($n = 9$; open squares) and rat A500V-ClC-2 + GlialCAM ($n = 8$; filled squares) in transfected HEK293T cells.

we hypothesise that the GlialCAM-mediated increase in currents in HEK293T cells could be partly due to altered gating characteristics of the mutant channel. We also verified that A500V-ClC-2 observed currents in the presence of GlialCAM were inhibited by iodide, indicating that they were not due to other chloride channels.

Effect of GlialCAM on the biochemical properties of ClC-2 mutants

To investigate if GlialCAM improves the stability of the cellular pool of human ClC-2 mutants, we used CHX chase analysis and immunoblotting. The modest improvement in the stability of A500V-ClC-2 upon GlialCAM co-expression in transfected HeLa cells was statistically not significant (Fig. 5*A*).

We used ELISA to measure the effect of GlialCAM on the PM levels of A500V-ClC-2. GlialCAM expression was ablated by siRNA transfection to minimise the effect of endogenous GlialCAM (Capdevila-Nortes *et al.* 2013), enabling us to assess the effect of a mutant GlialCAM in a null background. Interestingly, we found that GlialCAM slightly but significantly improved the PM density of both WT and mutant ClC-2, the PM density of A500V-ClC-2 remaining lower than that of the WT channel (Fig. 5*B*).

Next, we used ELISA to assess PM turnover of A500V-ClC-2 in the presence or absence of GlialCAM by measuring the disappearance kinetics of the anti-HA antibody-labelled channel complex from the PM. PM stability of ClC-2 is determined by its rate of endocytosis, the recycling of the endocytosed channel from early endosomes and the translocation of the internalised channel from endosomes to lysosomes where it is degraded. As expected for a subset of mutations eliciting conformational defects (Duarri *et al.* 2008), the mutant ClC-2 showed a significantly increased PM turnover (Fig. 5*C*). Co-expression of GlialCAM with A500V-ClC-2 decreased the PM turnover of A500V-ClC-2, having only a modest effect on WT ClC-2 (Fig. 5*C*) and indicating that restoration of A500V-ClC-2 PM expression could be attributed partly to its stabilisation at the PM.

Effect of GlialCAM on the subcellular localisation of ClC-2 mutants

GlialCAM has been reported to play a role in targeting ClC-2 to cell–cell junctions (Jeworutzki *et al.* 2012). Transient co-expression of human WT ClC-2 with GlialCAM in HeLa cells led to a co-localisation of both proteins in cell–cell junctions (Fig. 6*A*). By contrast, A500V-ClC-2 (Fig. 6*B*) displayed a diffuse perinuclear intracellular distribution when co-expressed with GlialCAM, the mutant ClC-2 and GlialCAM not showing any co-localisation.

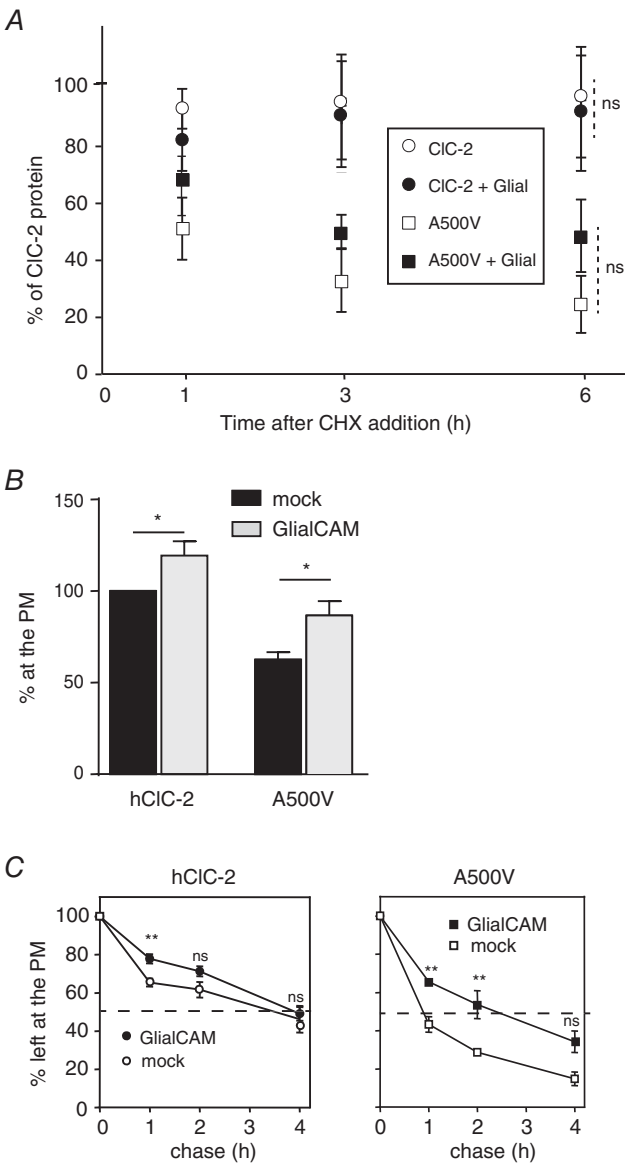

Figure 5. Effect of GlialCAM on ClC-2 protein stability and localisation
A, protein stability of WT ClC-2 and A500V-ClC-2 in the presence of GlialCAM. HeLa cells transfected with the indicated ClC-2 plasmids were incubated with the protein synthesis inhibitor CHX (100 mg ml^{-1}) for the indicated times (0, 1, 3 and 6 h). Cells were harvested, solubilised and analysed by western blotting. Quantification of proteins from four to five independent experiments is shown. For each group, the value at time 0 was normalised to 100%. Student's *t* test was used to compare data sets of WT ClC-2 or A500V-ClC-2 with and without GlialCAM. WT ClC-2 is indicated by open circles, WT ClC-2 + GlialCAM by filled circles, A500V-ClC-2 by open squares and A500V-ClC-2 + GlialCAM by filled squares. *B* and *C*, HeLa cells were depleted for GlialCAM and then co-transfected with WT GlialCAM or mock together with either WT or mutant ClC-2. PM density (*B*) and turnover (*C*) of ClC-2 variants were measured using cell surface ELISA. The dashed line in *C* indicates the value of 50% density at the PM. Data represent means ± SEM, $n = 3$–4 experiments. $^{*}P < 0.05$, $^{**}P < 0.01$, and ns, not significant (Student's *t* test) compared to mock at the indicated time point. PM, plasma membrane.

To confirm the mislocalisation of A500V-ClC-2 in rat primary astrocytes, we constructed adenoviral expression vectors encoding the WT and mutant ClC-2. While GlialCAM targeted WT ClC-2 to astrocyte–astrocyte junctions (Fig. 6*C*), it failed to suppress the mislocalisation of A500V-ClC-2 as we could not detect any co-localisation of GlialCAM and A500V-ClC-2 (Fig. 6*D*).

ClC-2 stabilisation at the PM requires GlialCAM targeting to cell–cell junctions

Our results suggested that the stabilisation of WT and mutant ClC-2 by GlialCAM may require GlialCAM accumulation in cell–cell junctions. To support this hypothesis, we performed pulse-labelling of ClC-2 fused to SNAP in the presence or absence of GlialCAM in transiently transfected HeLa cells. The addition of the SNAP-tag did not compromise ClC-2 targeting to cell–cell junctions (data not shown). The fluorescence intensity of ClC-2-SNAP decreased faster at the PM than at the cell–cell junctions (Fig. 7*A*), suggesting that GlialCAM stabilises ClC-2 at the cell surface when it is confined to cell–cell junctions.

We compared ClC-2 PM density and turnover in GlialCAM-depleted HeLa cells overexpressing the WT or Arg92Trp (R92W) GlialCAM variant, which has been identified in MLC2B patients (Lopez-Hernandez *et al.* 2011*a*). The R92W mutation impairs GlialCAM accumulation at cell–cell junctions (Lopez-Hernandez *et al.* 2011*b*). Interestingly, the PM density of WT ClC-2 was reduced by ~40% in cells expressing R92W-GlialCAM, while that of the mutant ClC-2 showed no significant changes (Fig. 7*B*). The importance of junctional targeting by GlialCAM was also demonstrated in experiments measuring the PM turnover of mutant ClC-2, with R92W-GlialCAM increasing the turnover of both WT ClC-2 and A500V-ClC-2 (Fig. 7*C*). Thus, junctional targeting by GlialCAM is required for ClC-2 stabilisation at the PM.

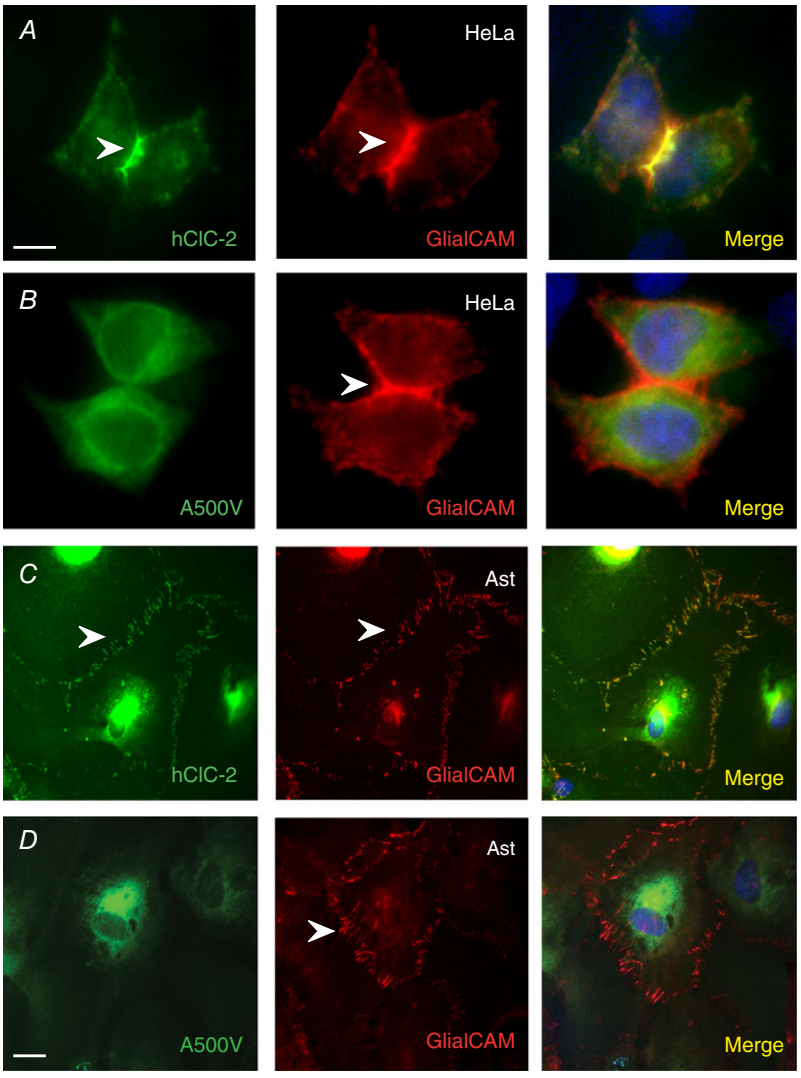

Figure 6. GlialCAM does not target ClC-2 mutants to cell–cell junctions
A and *B*, immunofluorescence of HeLa cells expressing WT ClC-2 (*A*) or A500V-ClC-2 (*B*) plus GlialCAM. GlialCAM is present in cell junctions (arrowheads) and co-localises with WT ClC-2 (*A*, right), but not with A500V-ClC-2 (*B*, right). Nuclei were stained with 4′,6-diamidino-2-phenylindole (blue). Scale bar, 20 μm. The signal exposure of the camera was increased to visualise A500V-ClC-2. Co-localisation of GlialCAM and ClC-2 (merge) was only observed for WT ClC-2. *C* and *D*, astrocytes were co-transduced with adenoviruses expressing WT ClC-2 (*C*) or A500V-ClC-2 (*D*) together with WT GlialCAM. Cells were fixed, permeabilised and then visualised by immunofluorescence (see 'Methods'). Co-localisation of ClC-2 (green) and GlialCAM (red) is shown in yellow (merge). Signal for A500V-ClC-2 was increased to visualise the mutant channel. Arrowheads point to contact sites between astrocytes. Images correspond to representative cells from three independent experiments. Scale bar, 20 μm. [Colour figure can be viewed at wileyonlinelibrary.com]

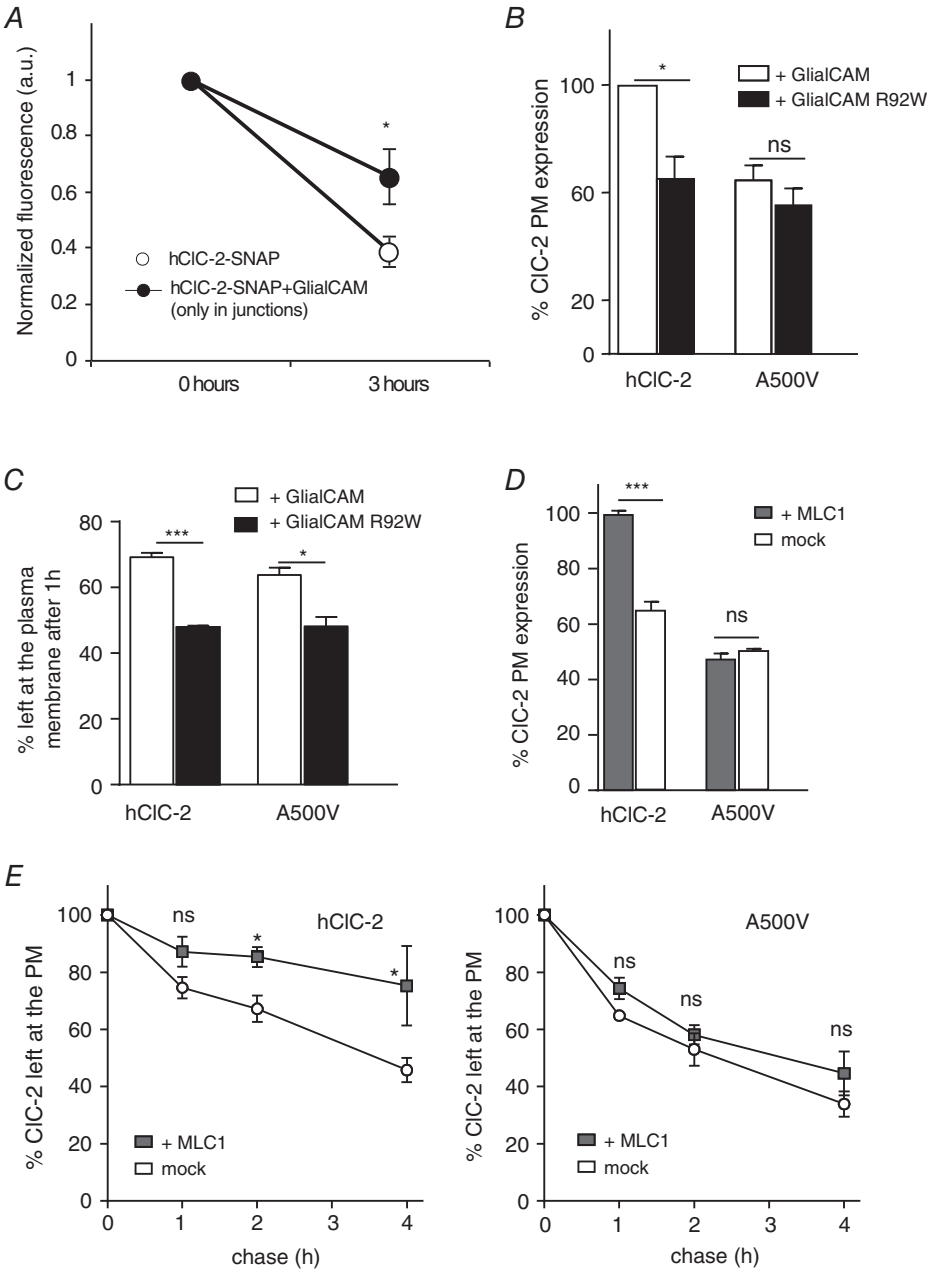

Figure 7. ClC-2 plasma membrane stabilisation depends on the presence of GlialCAM in cell–cell junctions

A, differences in the degradation rates of human WT ClC-2 at cell junctions or the PM were measured by SNAP pulse-labelling. Twenty-four hours after transfection, cells were pulse-labelled with SNAP-Cell® TMR-Star, washed and fixed 0 or 3 h after the pulse-labelling. The value at 3 h indicates the ratio of the mean fluorescence normalised to the value at time 0 for each group. The values are the result of 4 independent experiments with 8–12 cells in each assay. $^{*}P < 0.05$ compared to human ClC-2-SNAP alone (Student's *t* test). *B* and *C*, PM density (*B*) and turnover (*C*) after 1 h of WT ClC-2 and A500V-ClC-2 were determined by cell surface ELISA. HeLa cells were treated as in Fig. 5*B* and *C*, except that GlialCAM-depleted cells were now co-transfected with WT GlialCAM or the R92W mutant GlialCAM that is unable to localise to cell–cell junctions. Data are expressed as mean ± SEM. $^{*}P < 0.05$, $^{***}P < 0.001$, and ns, not significant (Student's *t* test) compared to WT GlialCAM-expressing cells. *D* and *E*, HeLa cells expressing GlialCAM were co-transfected with MLC1 or mock together with either WT ClC-2 or A500V-ClC-2. PM density (*D*) and turnover (*E*) of ClC-2 variants were measured using cell surface ELISA. $^{*}P < 0.05$, $^{***}P < 0.001$, and ns, not significant (Student's *t* test) compared to MLC1-expressing cells at the indicated time points.

GlialCAM, MLC1 and ClC-2 form a ternary complex in astrocytes (Sirisi *et al.* 2017), raising the possibility that MLC1 co-expression might also contribute to the stability of the complex. Indeed, MLC1 co-expression increased the PM density of WT, but not mutant ClC-2 in HeLa cells (Fig. 7*D*). This could be explained by the significantly reduced PM turnover of the WT ClC-2 in the presence of MLC1, with no changes observed for A500V-ClC-2 (Fig. 7*E*).

Discussion

We found that protein instability causes the impaired functional expression of the ClC-2 mutants associated with leukodystrophy. It is likely that ClC-2 mutations cause misfolding that then targets the mutants for endoplasmic reticulum- and endolysosomal-associated protein degradation. Thus, we suggest that *CLCN2*-related leukoencephalopathy (CC2L) should be considered a conformational disease. As ClC-2 is expressed in neurons, astrocytes and oligodendrocytes, it remains to be seen how a defect in these different cell types contributes to leukodystrophy. Our electrophysiological and biochemical studies of the A500V-ClC-2 mutant indicate that the mutation does not affect single-channel conductance, but changes the gating properties and steady-state expression of the channel at the PM. The mutant phenotype was influenced by the expression system and the method used to detect it at the PM, the defects being less severe in transfected cells than in *Xenopus* oocytes. This could be attributed to differences in the interaction between the channel and cytoskeleton, cellular proteostasis and the ambient temperature. It is important to mention here that detecting and quantifying protein levels at the PM by immunofluorescence can be difficult, especially if proteins are not concentrated in a specific domain, as is the case for cell–cell junctions.

GlialCAM increased the activity of A500V-ClC-2, although this never reached the activity levels of WT ClC-2. GlialCAM not only increased the open probability (P_{open}) of the mutant channel (Jeworutzki *et al.* 2014), but it also augmented the cell surface density (N) of the channel by reducing its turnover rate at the PM and, thus, enhancing its stability. This stabilisation depended on GlialCAM localisation to cell–cell junctions, since co-expression with an MLC-causing GlialCAM mutant, which shows reduced occurrence in junctions, elicited an increased turnover of ClC-2 at the PM. The interaction of GlialCAM with intracellular proteins, such as actin (Moh *et al.* 2009; Duarri *et al.* 2011), might help to tether ClC-2 either statically or dynamically to the PM. These results might also explain the reduced expression of ClC-2 in the cerebellum following GlialCAM knockout or the expression of a GlialCAM dominant mutant (G89S) (Hoegg-Beiler *et al.* 2014) with impaired targeting to cell–cell junctions (Lopez-Hernandez *et al.* 2011*b*).

Our results provide additional evidence supporting the role of GlialCAM as a subunit for MLC1 or ClC-2 (Barrallo-Gimeno *et al.* 2015). *In vitro* and *in vivo* data have shown that MLC1 expression at the PM depends on GlialCAM. Thus, loss of GlialCAM induces mislocalisation and a reduced expression of MLC1 in all brain regions (Capdevila-Nortes *et al.* 2013; Hoegg-Beiler *et al.* 2014). Moreover, GlialCAM stabilises the expression of MLC1 mutants by translocating them to cell–cell junctions (Capdevila-Nortes *et al.* 2013). By contrast, ClC-2 can translocate to the PM without GlialCAM, the loss of GlialCAM in mice reducing ClC-2 expression only in the cerebellum (Hoegg-Beiler *et al.* 2014). Moreover, GlialCAM and MLC1 co-localise completely in distal astrocytic processes, but GlialCAM and ClC-2 only partially (Depienne *et al.* 2013). We could not observe any co-localisation between GlialCAM and the mutant ClC-2 in HeLa cells and astrocytes. Considering all these results, we conclude that GlialCAM is an auxiliary subunit for ClC-2 without endoplasmic reticulum-chaperone activity (as for MLC1) and is primarily involved in stabilising and modulating ClC-2 turnover at the PM. Furthermore, we provide new evidence that GlialCAM, ClC-2 and MLC1 may form a ternary complex (Sirisi *et al.* 2017), as shown by MLC1 stabilising WT ClC-2 in the presence of GlialCAM.

We suggest that ClC-2 stabilisation at the PM by GlialCAM and MLC1 is partly due to the ability of these proteins to cluster at cell–cell junctions, since a GlialCAM mutant unable to accumulate in cell junctions could not stabilise ClC-2 at the PM, and MLC1, which increases the amount of GlialCAM at cell–cell junctions (Lopez-Hernandez *et al.* 2011*b*), could stabilise ClC-2 at the PM. Interestingly, although GlialCAM can interact with and functionally modify A500V-ClC-2, we did not observe any co-localisation in cell–cell junctions. In addition, MLC1 does not stabilise the mutant channel at the PM. We speculate that a critical concentration of complexes is required for localisation to cell–cell junctions and because the A500V-ClC-2 mutant is unstable, this critical concentration is not attained. In agreement with this hypothesis, Lopez-Hernandez *et al.* (2011*b*) reported that low levels of GlialCAM under a weak promoter (thymidine kinase) targeted fewer proteins (MLC1 or ClC-2) to cell junctions compared to that under a strong promoter (CMV).

In summary, based on our results and previously published data (Depienne *et al.* 2013), leukodystrophy is caused by a reduction in ClC-2-mediated currents resulting from mutations in the ClC-2 channel. Furthermore, our results indicate a new effect of GlialCAM-MLC1 on ClC-2 through its regulation of ClC-2 stability at the PM, explaining the defects observed in GlialCAM- and MLC1-knockout animals (Hoegg-Beiler *et al.*

2014). These data are important in understanding the pathophysiology of MLC and CC2L leukodystrophies.

References

Alvarez O, Gonzalez C & Latorre R (2002). Counting channels: a tutorial guide on ion channel fluctuation analysis. *Adv Physiol Educ* **26**, 327–341.

Barrallo-Gimeno A & Estévez R (2014). GlialCAM, a glial cell adhesion molecule implicated in neurological disease. *Adv Neurobiol* **8**, 47–59.

Barrallo-Gimeno A, Gradogna A, Zanardi I, Pusch M & Estévez R (2015). Regulatory-auxiliary subunits of CLC chloride channel-transport proteins. *J Physiol* **593**, 4111–4127.

Biasini M, Bienert S, Waterhouse A, Arnold K, Studer G, Schmidt T, Kiefer F, Gallo Cassarino T, Bertoni M, Bordoli L & Schwede T (2014). SWISS-MODEL: modelling protein tertiary and quaternary structure using evolutionary information. *Nucleic Acids Res* **42**, W252–W258.

Blanz J, Schweizer M, Auberson M, Maier H, Muenscher A, Hubner CA & Jentsch TJ (2007). Leukoencephalopathy upon disruption of the chloride channel ClC-2. *J Neurosci* **27**, 6581–6589.

Bosl MR, Stein V, Hubner C, Zdebik AA, Jordt SE, Mukhopadhyay AK, Davidoff MS, Holstein AF & Jentsch TJ (2001). Male germ cells and photoreceptors, both dependent on close cell-cell interactions, degenerate upon ClC-2 Cl^- channel disruption. *EMBO J* **20**, 1289–1299.

Capdevila-Nortes X, López-Hernández T, Apaja PM, López de Heredia M, Sirisi S, Callejo G, Arnedo T, Nunes V, Lukacs GL, Gasull X & Estévez R (2013). Insights into MLC pathogenesis: GlialCAM is an MLC1 chaperone required for proper activation of volume-regulated anion currents. *Hum Mol Genet* **22**, 4405–4416.

Cornejo I, Niemeyer MI, Zuniga L, Yusef YR, Sepulveda FV & Cid LP (2009). Rapid recycling of ClC-2 chloride channels between plasma membrane and endosomes: role of a tyrosine endocytosis motif in surface retrieval. *J Cell Physiol* **221**, 650–657.

Depienne C, Bugiani M, Dupuits C, Galanaud D, Touitou V, Postma N, van Berkel C, Polder E, Tollard E, Darios F, Brice A, de Die-Smulders CE, Vles JS, Vanderver A, Uziel G, Yalcinkaya C, Frints SG, Kalscheuer VM, Klooster J, Kamermans M, Abbink TE, Wolf NI, Sedel F & van der Knaap MS (2013). Brain white matter oedema due to ClC-2 chloride channel deficiency: an observational analytical study. *Lancet Neurol* **12**, 659–668.

Di Bella D, Pareyson D, Savoiardo M, Farina L, Ciano C, Caldarazzo S, Sagnelli A, Bonato S, Nava S, Bresolin N, Tedeschi G, Taroni F & Salsano E (2014). Subclinical leukodystrophy and infertility in a man with a novel homozygous CLCN2 mutation. *Neurology* **83**, 1217–1218.

Duarri A, Lopez de Heredia M, Capdevila-Nortes X, Ridder MC, Montolio M, Lopez-Hernandez T, Boor I, Lien CF, Hagemann T, Messing A, Gorecki DC, Scheper GC, Martinez A, Nunes V, van der Knaap MS & Estevez R (2011). Knockdown of MLC1 in primary astrocytes causes cell vacuolation: a MLC disease cell model. *Neurobiol Dis* **43**, 228–238.

Duarri A, Teijido O, Lopez-Hernandez T, Scheper GC, Barriere H, Boor I, Aguado F, Zorzano A, Palacin M, Martinez A, Lukacs GL, van der Knaap MS, Nunes V & Estevez R (2008). Molecular pathogenesis of megalencephalic leukoencephalopathy with subcortical cysts: mutations in MLC1 cause folding defects. *Hum Mol Genet* **17**, 3728–3739.

Estevez R, Schroeder BC, Accardi A, Jentsch TJ & Pusch M (2003). Conservation of chloride channel structure revealed by an inhibitor binding site in ClC-1. *Neuron* **38**, 47–59.

Giorgio E, Vaula G, Benna P, Lo Buono N, Eandi CM, Dino D, Mancini C, Cavalieri S, Di Gregorio E, Pozzi E, Ferrero M, Giordana MT, Depienne C & Brusco A (2017). A novel homozygous change of *CLCN2* (p.His590Pro) is associated with a subclinical form of leukoencephalopathy with ataxia (LKPAT). *J Neurol Neurosurg Psychiatry* **88**, 894–896.

Hanagasi HA, Bilgiç B, Abbink TEM, Hanagasi F, Tüfekçioğlu Z, Gürvit H, Başak N, van der Knaap MS & Emre M (2015). Secondary paroxysmal kinesigenic dyskinesia associated with CLCN2 gene mutation. *Parkinsonism Relat Disord* **21**, 544–546.

Hoegg-Beiler MB, Sirisi S, Orozco IJ, Ferrer I, Hohensee S, Auberson M, Gödde K, Vilches C, de Heredia ML, Nunes V, Estévez R & Jentsch TJ (2014). Disrupting MLC1 and GlialCAM and ClC-2 interactions in leukodystrophy entails glial chloride channel dysfunction. *Nat Commun* **5**, 3475.

Jentsch TJ (2015). Discovery of CLC transport proteins: cloning, structure, function and pathophysiology. *J Physiol* **593**, 4091–4109.

Jeworutzki E, Lagostena L, Elorza-Vidal X, López-Hernández T, Estévez R & Pusch M (2014). GlialCAM, a CLC-2 Cl^- channel subunit, activates the slow gate of CLC chloride channels. *Biophys J* **107**, 1105–1116.

Jeworutzki E, Lopez-Hernandez T, Capdevila-Nortes X, Sirisi S, Bengtsson L, Montolio M, Zifarelli G, Arnedo T, Muller CS, Schulte U, Nunes V, Martinez A, Jentsch TJ, Gasull X, Pusch M & Estevez R (2012). GlialCAM, a protein defective in a leukodystrophy, serves as a ClC-2 Cl^- channel auxiliary subunit. *Neuron* **73**, 951–961.

Leegwater PA, Yuan BQ, van der Steen J, Mulders J, Konst AA, Boor PK, Mejaski-Bosnjak V, van der Maarel SM, Frants RR, Oudejans CB, Schutgens RB, Pronk JC & van der Knaap MS (2001). Mutations of MLC1 (KIAA0027), encoding a putative membrane protein, cause megalencephalic leukoencephalopathy with subcortical cysts. *Am J Hum Genet* **68**, 831–838.

Lopez-Hernandez T, Ridder MC, Montolio M, Capdevila-Nortes X, Polder E, Sirisi S, Duarri A, Schulte U, Fakler B, Nunes V, Scheper GC, Martinez A, Estevez R & van der Knaap MS (2011*a*). Mutant GlialCAM causes megalencephalic leukoencephalopathy with subcortical cysts, benign familial macrocephaly, and macrocephaly with retardation and autism. *Am J Hum Genet* **88**, 422–432.

Lopez-Hernandez T, Sirisi S, Capdevila-Nortes X, Montolio M, Fernandez-Duenas V, Scheper GC, van der Knaap MS, Casquero P, Ciruela F, Ferrer I, Nunes V & Estevez R (2011*b*). Molecular mechanisms of MLC1 and GLIALCAM mutations in megalencephalic leukoencephalopathy with subcortical cysts. *Hum Mol Genet* **20**, 3266–3277.

Moh MC, Tian Q, Zhang T, Lee LH & Shen S (2009). The immunoglobulin-like cell adhesion molecule hepaCAM modulates cell adhesion and motility through direct interaction with the actin cytoskeleton. *J Cell Physiol* **219**, 382–391.

Pérez-Rius C, Gaitán-Peñas H, Estévez R & Barrallo-Gimeno A (2014). Identification and characterization of the zebrafish ClC-2 chloride channel orthologs. *Pflugers Arch* **467**, 1769–1781.

Pusch M, Steinmeyer K & Jentsch TJ (1994). Low single channel conductance of the major skeletal muscle chloride channel, ClC-1. *Biophys J* **66**, 149–152.

Scheper GC, van Berkel CG, Leisle L, de Groot KE, Errami A, Jentsch TJ & Van der Knaap MS (2010). Analysis of CLCN2 as candidate gene for megalencephalic leukoencephalopathy with subcortical cysts. *Genet Test Mol Biomarkers* **14**, 255–257.

Sirisi S, Elorza-Vidal X, Arnedo T, Armand-Ugón M, Callejo G, Capdevila-Nortes X, López-Hernández T, Schulte U, Barrallo-Gimeno A, Nunes V, Gasull X & Estévez R (2017). Depolarization causes the formation of a ternary complex between GlialCAM, MLC1 and ClC-2 in astrocytes: implications in megalencephalic leukoencephalopathy. *Hum Mol Genet* **26**, 2436–2450.

van der Knaap MS, Boor I & Estevez R (2012). Megalencephalic leukoencephalopathy with subcortical cysts: chronic white matter oedema due to a defect in brain ion and water homoeostasis. *Lancet Neurol* **11**, 973–985.

van der Knaap MS, Depienne C, Sedel F & Abbink TE (1993). CLCN2-related leukoencephalopathy. In *GeneReviews*, ed. Pagon RA, Adam MP, Ardinger HH, Wallace SE, Amemiya A, Bean LJH, Bird TD, Ledbetter N, Mefford HC, Smith RJH & Stephens K. University of Washington, Seattle, https://www.ncbi.nlm.nih.gov/books/NBK326661/.

Zeydan B, Uygunoglu U, Altintas A, Saip S, Siva A, Abbink TEM, van der Knaap MS & Yalcinkaya C (2017). Identification of 3 novel patients with CLCN2-related leukoencephalopathy due to CLCN2 mutations. *Eur Neurol* **78**, 125–127.

Zuniga L, Niemeyer MI, Varela D, Catalan M, Cid LP & Sepulveda F V (2004). The voltage-dependent ClC-2 chloride channel has a dual gating mechanism. *J Physiol* **555**, 671–682.

Additional information

Competing interests

The authors declare no conflict of interest.

Author contributions

H.G.-P. performed the biochemical and electrophysiological experiments in *Xenopus* oocytes plus some biochemical studies in HeLa cells, while P.M.A. performed surface analysis of HeLa cells. T.A. performed biochemical experiments in HeLa cells and X.E.-V. conducted SNAP pulse-labelling of ClC-2 in HeLa cells. A.C., D.S. and X.G. performed patch-clamp analyses in HEK293T cells. G.L.L. and R.E. supervised the project and wrote the manuscript with input from all the authors. All authors have approved the final version of the manuscript and agree to be accountable for all aspects of the work. All persons designated as authors qualify for authorship, and all those who qualify for authorship are listed. All work was done at the University of Barcelona or McGill University (Canada).

Funding

This study was supported by SAF 2015-70377-R (R.E.), CIBERER-ERARE2 (R.E. and G.L.), the ELA Foundation 2012–014C2 grant (R.E.), 2014 SGR 1178 (R.E.), Instituto de Salud Carlos III FIS PI14/00141 (X.G.), RETIC RD12/0034/0003 and RD16/0008/0014 (X.G.), 2014 SGR 1165 (X.G.), BFU2014-57562-P (D.S.) and the Canadian Institute of Health Research and the Canada Foundation for Innovation (G.L.). G.L. is a Canada Research Chair and RE a recipient of an ICREA Academia prize.

Acknowledgements

We thank Michael Pusch and Alejandro Barrallo-Gimeno for their helpful comments on the manuscript.